Optical Fiber Technology 60 (2020) 102316

Contents lists available at ScienceDirect

Optical Fiber Technology

journal homepage: www.elsevier.com/locate/yofte

Ultra-broadband and highly sensitive surface plasmon resonance sensor based on four-core photonic crystal fibers

Jianfei Liao[a], Ziping Ding[a], Yingmao Xie[a], Xinghua Wang[a], Zekai Zeng[a], Tianye Huang[b,*]

[a] College of Physics and Electronic Information, Gannan Normal University, Ganzhou 341000, China
[b] School of Mechanical Engineering and Electronic Information, China University of Geosciences (Wuhan), Wuhan 430074, China

ARTICLE INFO

Keywords:
Photonic crystal fibers
Surface plasmon resonance
Fiber optics sensor
Refractive index sensor

ABSTRACT

An ultra-broadband surface plasmon resonance (SPR) sensor with high sensitivity adopting four-core photonic crystal fiber is designed. The impacts of fiber structure parameters on the sensing performance are theoretically studied in detail. The investigation results demonstrate that, the average wavelength sensitivity of our proposed sensor is up to 1.135×10^4 nm/refractive index unit (RIU) within the ultra-broad wavelength range of 1.548–2.683 μm when the refractive index (RI) of analyte varies in a large range of 1.423–1.523. Furthermore, the maximum amplitude sensitivity of 550 RIU^{-1} is achieved if RI changes from 1.423 to 1.433. Therefore, the proposed sensor can work both in the telecommunication window, and the mid-infrared wavelength regime.

1. Introduction

Recently, surface plasmon resonance (SPR) sensors have attracted more and more research interests and extensively applied in environment monitoring, food safety control and liquid detection thanks to its several advantages such as high sensitivity, label-free and real-time detection [1–3]. The earliest SPR sensor always contains a coupling prism with a film of metal-deposited [4,5]. Nevertheless, prim-based SPR sensors have several obvious drawbacks including bulky, costly integration, and so on [6]. In order to overcome these drawbacks, conventional optical fiber is employed to replace the prism because of its spatial miniaturization, low cost, anti-electromagnetic interference, and higher sensitivity. Nowadays, various of fiber-based SPR sensors are reported [7–10]. In particularly, Sharma et al. proposed a new type of plasmonic sensor based on optical fiber grating for salivary cortisol sensing [11]. The simulation results show that in angular interrogation mode (AIM), the average limit-of-detection (LOD) of SiO_2 and SiC-based sensor designs are 9.9 pg/mL and 9.8 pg/mL, respectively. If the intensity interrogation method in place of AIM is considered, the average LOD can be as high as 22.6 pg/mL and 68.17 pg/mL, respectively. Furthermore, another type of 2D material/metal carbide based optical fiber SPR probe is also proposed by Sharma et al. for ultrasensitive cortisol detection [12]. The results reveal that the $Ti_3C_2O_2$-based probe can offer superior overall sensing performance with a LOD 15.7 fg/mL. But the fiber used in these sensors is always tapered or polished, which limits the design flexibility and sensitivity improvement. Compared with the traditional optical fiber, photonic crystal fiber (PCF) is much more flexible and allows extension of the operation range.

Up till now, various of PCF-SPR sensors such as H-shaped PCF-SPR sensors [13,14], D-shaped PCF-SPR sensors [15–17], slotted PCF-SPR sensors [18,19], square lattice PCF-SPR sensors [20] and muti-core PCF-SPR sensors [21–23] have been proposed. In these researches, most of PCF-based SPR sensors work in the visible or near-infrared wavelength region [24,25]. For the purpose of further expanding the application, Liu et al. proposed a simple mid-infrared PCF-based SPR sensor [26]. The proposed sensor can work in the mid-infrared wavelength range from 2550 nm and 2900 nm by using two open-ring channels structure. The simulation results indicate that an average sensitivity of 5500 nm/refractive index unit (RIU) is realized when the refractive index (RI) of the analyte (n_a) lies in (1.23, 1.29). Moreover, the maximum refractive-index resolution is up to 7.69×10^{-6}. However, to our best knowledge, PCF-based SPR sensors, which can operate in both the near-infrared and mid-infrared wavelength region, have seldom been rarely reported.

In this paper, an ultra-broadband PCF-SPR sensor with high sensitivity is proposed. Through optimizing the sensor structure parameters, an average sensitivity of 1.135×10^4 nm/ RIU within the ultra-broad wavelength range of 1.548–2.683 μm is obtained when n_a lies in (1.423, 1.523). On the other hand, the maximum amplitude sensitivity, wavelength sensitivity and refractive index resolution are up to 549.6 RIU^{-1}, 1.25×10^4 nm/RIU, 8×10^{-6} RIU, respectively.

* Corresponding author.
E-mail address: tianye_huang@163.com (T. Huang).

https://doi.org/10.1016/j.yofte.2020.102316
Received 21 May 2020; Received in revised form 12 July 2020; Accepted 15 July 2020
1068-5200/ © 2020 The Authors. Published by Elsevier Inc. This is an open access article under the CC BY-NC-ND license (http://creativecommons.org/licenses/BY-NC-ND/4.0/).

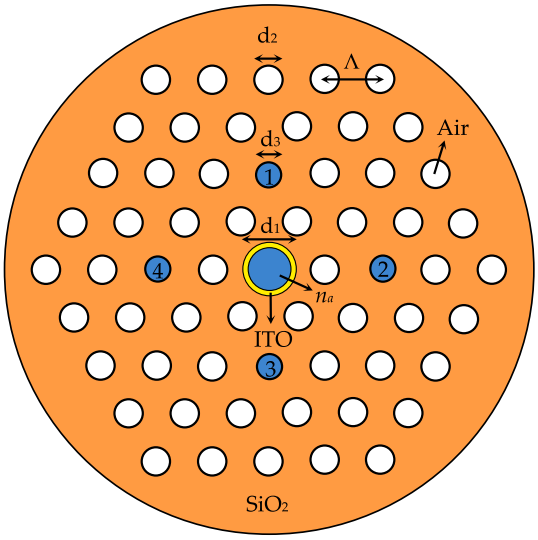

Fig. 1. Geometry of our designed four-core PCF SPR sensor.

2. Theoretical model

The geometry of the four-core PCF SPR sensor is presented in Fig. 1. The designed PCF includes four layers of circle holes arranged in a regular triangular lattice. There are four small air holes infiltrated with the analyte in the center of four fiber core regions, which are labeled 1, 2, 3, 4 in sequence. Note that these four small air holes infiltrated with the analyte in the center of four fiber core regions can effectively adjust the mode effective RI of the fundamental core-guided mode, which can help our proposed sensor fulfill the resonance condition in a large n_a range, and then the proposed sensor can work both in near-infrared and mid-infrared wavelength regime. A single analyte channel structure is adopted in proposed sensor to eliminate the distribution between adjacent analyte channels. Moreover, we use indium tin oxide (ITO) as plasmon active metal material instead of other noble metals including silver and gold. The main parameters of PCF include the diameter of the cladding hole d_2, the lattice pitch Λ, the diameter of the central channel hole d_1, the thickness of the ITO layer t, and the diameter of the hole filled analyte in the fiber core d_3. As the background materials of PCF, the refractive index of silica is calculated from Sellmeier equation [27]. Meanwhile, the relative dielectric constant of ITO can be obtained using the Drude model [15]. The RI of analyte is n_a. Note that our designed PCF with four cores can be drew by employing the stack-and-draw technology. After doing that, we can adopt the high pressure chemical vapor deposition method to deposit ITO layer, and infiltrate the channel hole and the four small holes located in the core central region with analyte. Therefore, our proposed PCF SPR senor should be fabricated.

In order to study the sensing property of our designed sensor accurately, full vector finite element method with the PML boundary condition is applied, and the confinement lossCL, wavelength sensitivity S_λ and amplitude sensitivity S_a are calculated using the following equations [28].

$$CL(dB/cm) = 8.686 \times (2\pi/\lambda)\mathrm{Im}(n_{eff}) \times 10^4 \quad (1)$$

$$S_\lambda(nm/RIU) = \Delta\lambda_{peak}(n_a)/\Delta n_a \quad (2)$$

$$S_a = -(\Delta CL/\Delta n_a)/CL_{initial} \quad (3)$$

where$\lambda$and $\mathrm{Im}(n_{eff})$ stand for the wavelength and the imaginary part of the n_{eff}, respectively. $\Delta\lambda_{peak}$ is the change of resonance wavelength while Δn_a is the RI variation. ΔCL denotes the confinement loss changes and $CL_{initial}$ represents the initial confinement loss.

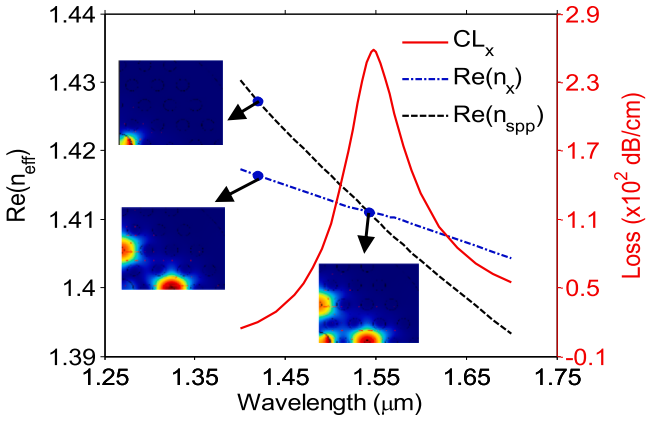

Fig. 2. The real parts of the effective indices and confinement loss with n_a = 1.423. Insets are the mode field distributions of the SPP and x-polarized fundamental modes.

3. Simulation results and discussion

Because of the geometrical symmetry, both the orthogonal polarization fundamental core-guided modes can induce surface plasmon polaritons (SPPs) identically. Therefore, we only study the coupling resonance characteristics between the x-polarized fundamental core-guided mode and the SPP mode in this paper. Fig. 2 shows the modal distribution and phase matching characteristic of the proposed SPR sensor with fiber parameters d_1 = 2 μm, d_2 = 1 μm, d_3 = 0.5 μm, t = 50 nm, and Λ = 2 μm when n_a is equal to1.423. One can find that the real part of the n_{eff} of the two modes (Re(n_x), Re(n_{spp})) decreases with wavelength increasing, but Re(n_{spp}) decreases much faster than Re(n_x), and then the two curves intersect at the wavelength of 1.548 μm, which proves that the resonance condition between the x-polarized and SPP modes is fulfilled at 1.548 μm. We can attribute this phenomenon that electromagnetic wave phase is influenced by SPR. Furthermore the corresponding fundamental core mode shows a sharp loss peak at the wavelength of 1.548 μm, which means that the two modes have strong resonance coupling. Therefore, most of the electromagnetic wave energy of the fundamental mode is coupled into SPP mode, which is proved by the inset. On the contrary, the core mode at 1.42 μm is mostly distributed in the fiber core and the SPP mode at 1.42 μm is well confined at the surface of ITO.

Firstly, we investigate the impact of n_a on the peak wavelength of proposed sensor with parameters d_1 = 2 μm, d_2 = 1 μm, d_3 = 0.5 μm, t = 50 nm, and Λ = 2 μm. Fig. 3a shows that the peak wavelength moves to long wavelength side with n_a increasing. For example, the peak wavelength is 1.548 μm at n_a = 1.423 while the resonance wavelength increases to 2.683 μm at n_a = 1.523. The main reason is that a larger n_a leads to larger Re(n_{spp}), so the peak wavelength moves to long wavelength side. Therefore, our proposed PCF SPR sensor can operate within an ultra-broadband wavelength range from near-infrared region to mid-infrared region. Fig. 3b shows the dependence of the resonance wavelength on n_a. It can be found that the linearity between the peak wavelength and n_a is good. In order to obtain the average wavelength sensitivity, the linear fitting between the peak wavelength and n_a is given in Fig. 3c. The linear regression equation is obtained as $\lambda(\mu m) = 11.350 n_a - 15.113$. From this equation, we can learn that the average wavelength sensitivity of our proposed sensor is as high as 1.135 × 10^4 nm/RIU when n_a varies from 1.423 to 1523. The maximum wavelength sensitivity is 1.25 × 10^4 nm/RIU if n_a changes from 1.473 to 1.483. Assuming that wavelength resolution of the instrument is 0.1 nm, the RI resolution is as high as 8 × 10^{-6} RIU.

Since surface plasmon wave is susceptible to the thickness of metallized layer when SPR occurs. In this section, we investigate the effect of t on the peak wavelength of the sensor with fiber parameters

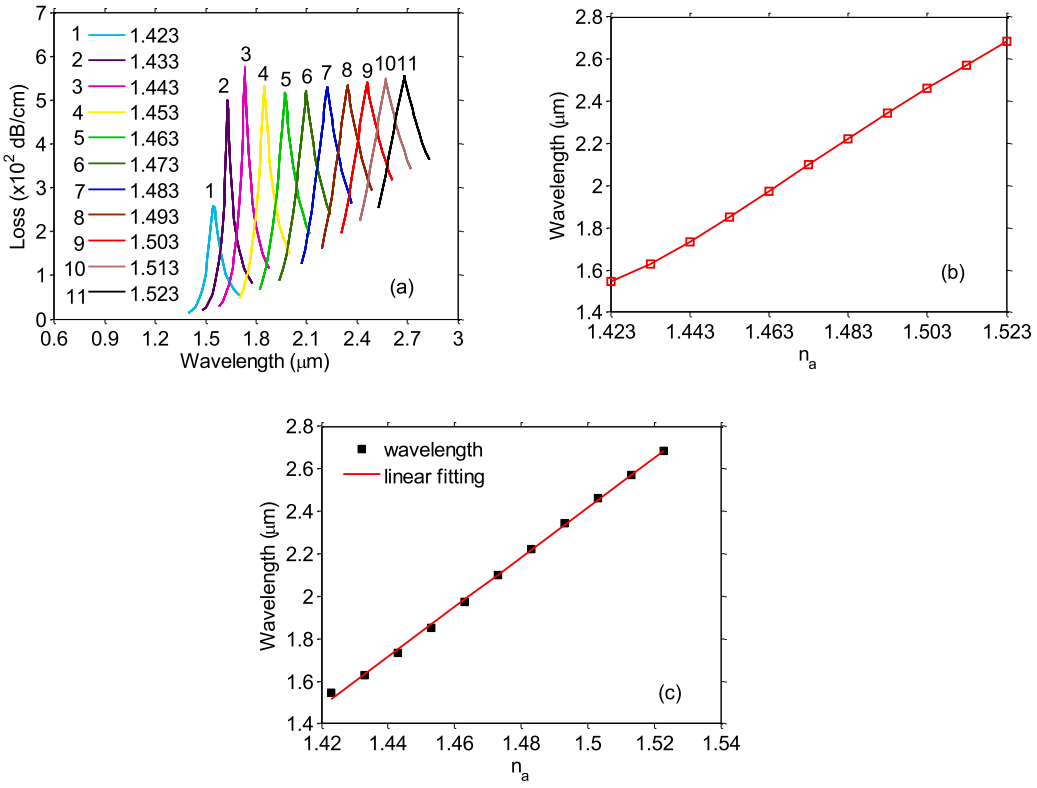

Fig. 3. Loss of fundamental core mode (a), peak wavelength (b), and linear fitting line of the resonance wavelength versus n_a (c) by changing n_a from 1.423 to 1.523.

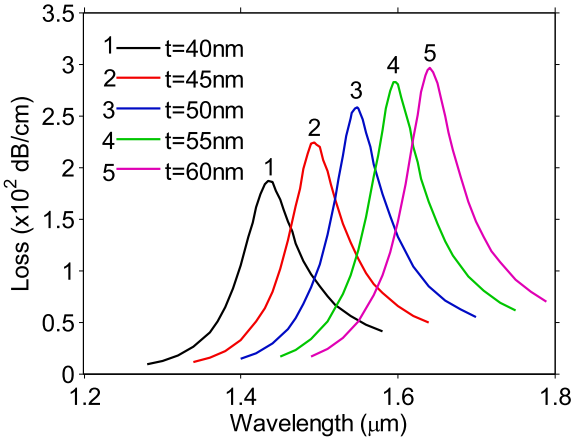

Fig. 4. The impact of t on the loss of x-polarized fundamental mode.

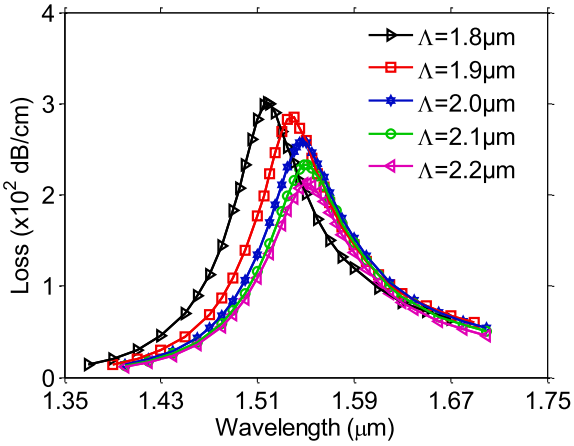

Fig. 5. The lattice effect of Λ on the loss of x-polarized mode for proposed sensor with d_1 = 2 μm, d_2 = 1 μm, d_3 = 0.5 μm, t = 50 nm, and n_a = 1.423.

d_1 = 2 μm, d_2 = 1 μm, d_3 = 0.5 μm, Λ = 2 μm, n_a = 1.423, and the calculation results are given in Fig. 4. One can find that the peak wavelength of fiber core mode moves to long wavelength when t increases from 40 nm to 60 nm. Moreover, the peak loss of proposed sensor increases with the increment of ITO film thickness, which is in agreement with previous reports [21]. This phenomenon indicates that, when t increases, the resonance intensity between the core mode and SPP mode becomes stronger, and then more electromagnetic energy of fiber fundamental mode is coupled into SPP mode.

Besides metal thickness, the lattice pitch Λ and the hole diameter d_3 can also modify the sensing performance. Hence, we investigate the effect of Λ on the loss of core mode and the results are given in Fig. 5. The resonance peak moves to long wavelength side and the drift distance shrinks with the lattice pitch Λ increasing. The corresponding peak loss also shows a downward trend because the resonance strength between the core mode and SPP mode weakens with the increment of the lattice pitch. Fig. 6 displays the impact of d_3 on the loss of the x-polarized fundamental mode. We can find that the increase of d_3 leads to red-shift of the peak wavelength. Meanwhile, the loss peak value shows an upward trend. The main reason is that the resonance intensity of these two modes is enhanced when the air hole diameter d_3 increases. In addition, the loss of our designed sensor reaches to the maximum at 1.575 μm when d_3 = 0.9 μm. This indicates that it is the optimal diameter.

Fig. 7 demonstrates the influences of the thickness of ITO film and the lattice pitch on the wavelength sensitivity when n_a increases from 1.423 to 1.523. In Fig. 7a, other fiber parameters are set d_1 = 2 μm, d_2 = 1 μm, d_3 = 0.5 μm, and Λ = 2 μm. One can learn from this figure that when n_a increases from 1.423 to 1.473, the wavelength sensitivity increases with n_a increasing for the same t. However, if n_a increases from 1.473 to 1.523, the wavelength sensitivity decreases with n_a

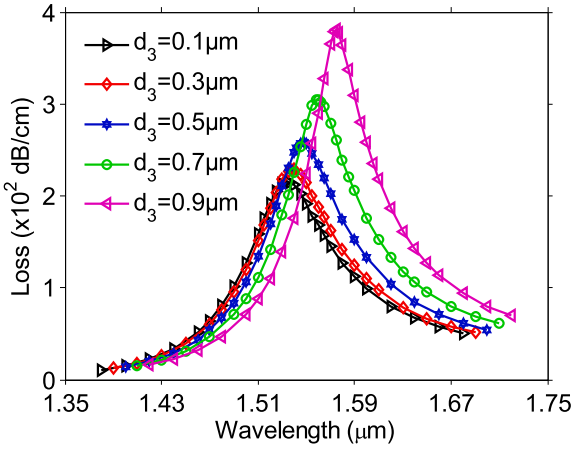

Fig. 6. The impact of d_3 on the loss of x-polarized mode for proposed sensor with $d_1 = 2$ μm, $d_2 = 1$ μm, $t = 50$ nm, $\Lambda = 2$ μm, and $n_a = 1.423$.

increasing for the same t. Furthermore, the wavelength sensitivity decreases with t increasing for the same n_a change except when n_a increases from 1.423 to 1.433. It should be noted that the proposed sensor has the same wavelength sensitivity at $t = 55$ nm and $t = 60$ nm when n_a increases from 1.423 to 1.433. This is because the coupling efficiency between the fundamental core-guided mode and the SPP mode remains unchanged when t increases from 55 nm to 60 nm. The similar phenomena is reported in previous works as well [15,28]. As seen from Fig. 7(b), the influence of the lattice pitch on the wavelength sensitivity is similar to that of t with fiber parameters of $d_1 = 2$ μm, $d_2 = 1$ μm, $d_3 = 0.5$ μm, and $t = 50$ nm. The wavelength sensitivity increases for the same Λ when n_a increases from 1.423 to 1.473. Meanwhile, it decreases for the same Λ when n_a increases from 1.423 to 1.473.

Finally, we study the influences of the thickness of ITO film and the lattice pitch on the amplitude interrogation. Note that the amplitude sensitivity can be calculated by using equation (3). Fig. 8a depicts the amplitude sensitivity for different the thickness of ITO film with the fiber parameters of $d_1 = 2$ μm, $d_2 = 1$ μm, $d_3 = 0.5$ μm, and $\Lambda = 2$ μm. It is clear that the amplitude sensitivity exists a downward trend and the amplitude sensitivity curves shift towards longer wavelength with the increment of t. The maximum amplitude sensitivity is up to 433 RIU^{-1} if $t = 45$ nm. Fig. 8b demonstrates the dependences of amplitude sensitivity on Λ with the fiber parameters of $d_1 = 2$ μm, $d_2 = 1$ μm, $d_3 = 0.5$ μm, and $t = 50$ nm. The variation trend of the maximum amplitude sensitivity is similar to that of the metal layer thickness, the maximum amplitude sensitivity of 550 RIU^{-1} is achieved when $\Lambda = 1.9$ μm. Moreover, the amplitude sensitivity curves at $\Lambda = 1.8$ μm and 1.9 μm are nearly the same. The main reason is that when the lattice pitch increases from 1.8 μm to 1.9 μm, the coupling efficiency between the fundamental core-guided mode and the SPP mode almost keeps unchanged but the resonance wavelength shifts toward longer wavelength, which is verified by Fig. 5. Such phenomena also exists in other works [15,29]. To estimate the sensing property of our designed sensor, a comparison of other multi-core PCF-based SPR sensor performances including the detection RI range, the resonance wavelength range, the maximum wavelength sensitivity, the average wavelength sensitivity and the maximum amplitude sensitivity is given in Table 1. As shown in Table 1, we can find that the detection RI range of our proposed sensor is much larger than that of these multi-core PCF SPR sensors except six-core PCF SPR sensor. Furthermore, compared with these multi-core PCF SPR sensors, the proposed sensor not only possesses a higher sensing sensitivity but also can operate within an ultra-broadband wavelength range from near-infrared region to mid-infrared region.

4. Conclusion

In summary, a simple ultra-broadband SPR sensor with high sensitivity by employing four-core PCF structure is proposed and thoroughly studied. Our numerical results reveal that the fiber structure parameters can efficiently affect the sensing performance. By properly adjusting the fiber structure parameters, the maximum wavelength and amplitude sensitivities are as high as 1.25×10^4 nm/RIU and 550 RIU^{-1}, respectively. Moreover, the resonance wavelength can operate in an ultra-broad wavelength range of 1.548–2.683 μm, which is suitable for both near-infrared and mid-infrared detection.

CRediT authorship contribution statement

Jianfei Liao: Conceptualization, Methodology, Writing - original draft, Funding acquisition. **Ziping Ding:** Formal analysis, Investigation, Data curation. **Yingmao Xie:** Supervision, Funding acquisition. **Xinghua Wang:** Data curation, Visualization. **Zekai Zeng:** Validation. **Tianye Huang:** Writing - review & editing, Project administration.

Declaration of Competing Interest

The authors declare that they have no known competing financial interests or personal relationships that could have appeared to influence the work reported in this paper.

Acknowledgements

This research was funded by the National Natural Science Foundation of China (Project No. 61765003); Natural Science Foundation of Jiangxi province (Project No. 20181BAB202029); Educational Committee Science Foundation of Jiangxi Province (Project No. GJJ18075) and Graduate Innovation Foundation of Gannan Normal University (Project No. YCX19A043).

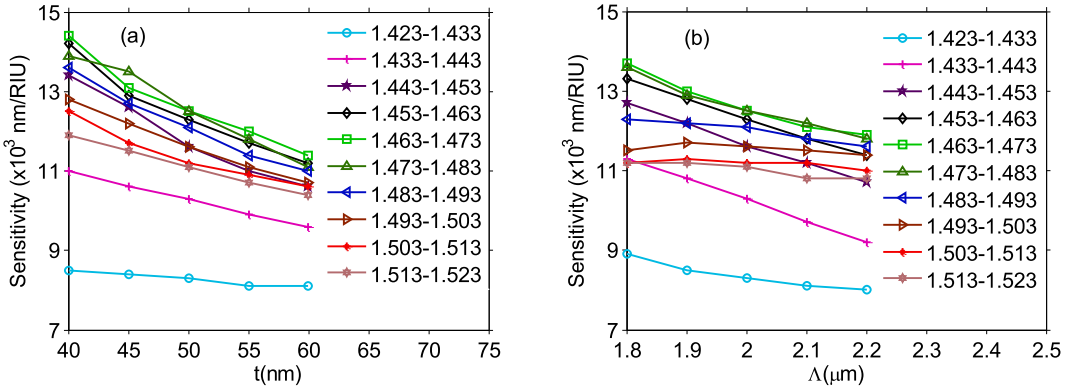

Fig. 7. The impacts of the thickness of ITO film (a) and the lattice pitch (b) on the wavelength sensitivity with n_a increasing from 1.423 to 1.523.

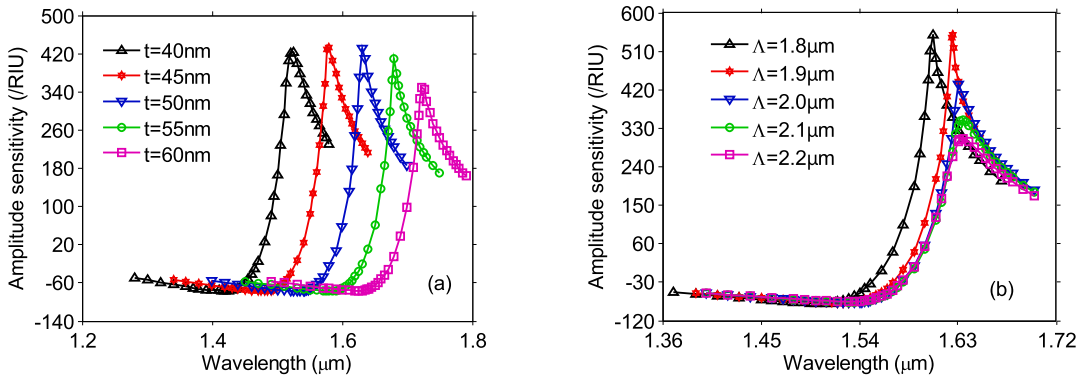

Fig. 8. The impacts of the thickness of ITO film (a) and the lattice pitch (b) on the amplitude sensitivity with n_a increasing from 1.423 to 1.433.

Table 1
Comparison of other multi-core PCF-based SPR sensor performances.

Sensor Type	RI Range (RIU)	Res. Wav. Ran. (μm)	Max. Wav. Sens. (nm/RIU)	Ave. Wav. Sens. (nm/RIU)	Max. Amp. Sens. (RIU^{-1})	Ref.
Two-core PCF sensor	1.46–1.49	~0.99–1.13	3000	2390	418	[21]
Three-core PCF sensor	1.33–1.40	~0.59–0.85	N/A	3435	N/A	[22]
Six-core PCF sensor	1.33–1.42 1.43–1.53	0.40–0.80 0.80–1.85	N/A	2929.39 9231.27	N/A	[23]
This work	1.423–1.523	1.548–2.683	12,500	11,350	550	N/A

References

[1] A.K. Sharma, A.K. Pandey, B. Kaur, A review of advancements (2007–2017) in plasmonics-based optical fiber sensors, Opt. Fiber Technol. 43 (2018) 20–34.
[2] Y. Zhao, M. Lei, S. Liu, Q. Zhao, Smart hydrogel-based optical fiber SPR sensor for pH measurements, Sens. Actuators B Chem. 261 (2018) 226–232.
[3] M.S. Aruna Gandhi, S. Chu, K. Senthilnathan, P.R. Babu, K. Nakkeeran, Q. Li, Recent advances in plasmonic sensor-based fiber optic probes for biological applications, Appl. Sci. 9 (2019) 949.
[4] P. Singh, S.P.R. Biosensors, Historical Perspectives and Current Challenges, Sens. Actuators B Chem. 229 (2016) 110–130.
[5] W.W. Lam, L.H. Chu, C.L. Wong, Y.T. Zhang, A surface plasmon resonance system for the measurement of glucose in aqueous solution, Sens. Actuators B Chem. 105 (2005) 138–143.
[6] E. Klantsataya, P. Jia, H. Ebendorff-Heidepriem, T.M. Monro, A. Francois, Plasmonic fiber optic refractometric sensors: From conventional architectures to recent design trends, Sensors17 (2016) 12.
[7] X. Xi, J. Xu, S. Li, J. Song, W. Yang, Y. Sun, S. Jiang, Y. Han, X. Fan, An Au nanofilm-graphene/D-type fiber surface plasmon resonance sensor for highly sensitive specificity bioanalysis, Sensors 20 (2020) 991.
[8] K. Shah, N.K. Sharma, V. Sajal, SPR based fiber optic sensor with bi layers of indium tin oxide and platinum: A theoretical evaluation, Optik 135 (2017) 50–56.
[9] J.K. Nayak, R. Jha, Numerical simulation on the performance analysis of a graphene-coated optical fiber plasmonic sensor at anti-crossing, Appl. Opt. 56 (2017) 3510–3517.
[10] D. Paul, S. Dutta, R. Biswas, LSPR enhanced gasoline sensing with a U-bent optical fiber, J. Phys. D:Appl. Phys. 49 (2016) 305104.
[11] A.K. Pander, A.K. Sharma, C. Marques, On the application of SiO_2/SiC grating on Ag for high-performance fiber optic plasmonic sensing of cortisol concentration, Materials 13 (2020) 1623.
[12] A.K. Sharma, B. Kaur, C. Marques, Simulation and analysis of 2D material/metal carbide based fiber optic SPR probe for ultrasensitive cortisol detection, Optik 218 (2020) 164891.
[13] H. Han, D. Hou, L. Zhao, N. Luan, L. Song, Z. Liu, Y. Lian, J. Liu, Y. Hu, A large detection-range plasmonic sensor based on an H-shaped photonic crystal fiber, Sensor 20 (2020) 1009.
[14] T. Li, L. Zhu, X. Yang, X. Lou, L. Yu, A refractive index sensor based on H-shaped photonic crystal fibers coated with Ag-graphene layers, Sensor 20 (2020) 741.
[15] T. Huang, Highly sensitive SPR sensor based on D-shaped photonic crystal fiber coated with Indium Tin Oxide at near-infrared wavelength, Plasmoncis 12 (2017) 583–588.
[16] J.N. Dash, R. Jha, On the performance of graphene-based D-shaped photonic crystal fiber biosensor using surface plasmon resonance, Plasmonics 10 (2015) 1123–1131.
[17] N.N. Luan, L. Zhao, Y.D. Lian, S.Q. Lou, A high refractive index plasmonic sensor based on D-shaped photonic crystal fiber with laterally accessible hollow-core, IEEE Photonics J. 10 (2018) 1–7.
[18] R. Otupiri, E. Akowuah, S. Haxha, Multi-channel SPR biosensor based on PCF for multi-analyte sensing applications, Opt. Express 23 (2015) 15716–15727.
[19] S.I. Azzam, M.F.O. Hameed, R.E.A. Shehata, A. Heikal, S. Obayya, Multichannel photonic crystal fiber surface plasmon resonance based sensor, Opt. Quantum. Electron. 48 (2016) 1–11.
[20] C. Liu, W. Su, F. Wang, X. Li, Q. Liu, H. Mu, T. Sun, P.K. Chu, Birefringent PCF-based SPR sensor for a broad range of low refractive index detection, Photo. Technol. Lett. 30 (2018) 1471–1474.
[21] A.A. Rifat, G.A. Mahdiraji, D.M. Chow, Y.G. Shee, R. Ahmed, F.R.M. Adikan, Photonic crystal fiber-based surface plasmon resonance sensor with selective analyte channels and graphene-silver deposited core, Sensor 15 (2015) 11499–11510.
[22] K. Tong, F. Wang, M. Wang, P. Dang, Y. Wang, Three-core photonic crystal fiber surface plasmon resonance sensor, Opt. Fiber Technol. 46 (2018) 306–310.
[23] B. Shuai, L. Xia, Y. Zhang, D. Liu, A multi-core holey fiber based plasmonic sensor with large detection range and high linearity, Opt. Express 20 (2012) 5974–5986.
[24] J. Liu, H.Q. Liang, B. Liu, X.D. He, Z.P. Chen, Abnormal sensing properties of surface plasmon resonance sensor based on photonic crystal fibers, Opt. Fiber Technol. 48 (2019) 248–252.
[25] Z. Fan, Surface plasmon resonance refractive index sensor based on photonic crystal fiber covering nano-ring gold film, Opt. Fiber Technol. 50 (2019) 194–199.
[26] C. Liu, L. Yang, X. Lu, Q. Liu, F. Wang, J. Lv, T. Sun, H. Mu, P.K. Chu, Mid-infrared surface plasmon resonance sensor based on photonic crystal fibers, Opt. Express 26 (2017) 14227–14237.
[27] G. Ghosh, M. Endo, T. Iwasaki, Temperature-dependent Sellmeier coefficients and chromatic dispersions for some optical fiber glasses, J. Lightwave Technol. 12 (1994) 1338–1342.
[28] E. Haque, M.A. Hossain, F. Ahmed, Y. Namihira, Surface plasmon resonance sensor based on modified D-shaped photonic crystal fiber for wider range of refractive index detection, IEEE Sens. J. 18 (2018) 8278–8293.
[29] A. Hassani, M. Skorobogatiy, Design criteria for microstructured-optical-fiber-based surface-plasmon- resonance sensors, J. Opt. Soc. Am. B 24 (2007) 1423–1429.